

Evaluation of microphysics schemes in the WRF-ARW model for numerical wind forecast in José Martí International Airport.

Patricia Coll-Hidalgo^{1,*}, Albenis Pérez-Alarcón^{2,3}, Pedro Manuel González-Jardines⁴

¹ Department of Meteorology, Higher Institute of Technologies and Applied Sciences, University of Havana, Cuba,

² Environmental Physics Laboratory (EPhysLab), CIM-UVigo, Universidade de Vigo, 32004 Ourense, Spain,

³ Cuban Corporation of Air Navigation

* Correspondence: pcoll@instec.cu; Tel.: +53-5-803-1337 (P.C.-H.)

Received: date; Accepted: date; Published: date

Abstract: A sensitivity study was developed with Lin, Morrison 2-moment, WSM5 (WRF Single-Moment 5-class), and WSM6 (WRF Single-Moment 6-class) microphysics schemes available in the WRF-ARW (Weather Research and Forecasting-Advanced Research WRF) for the numerical forecast of the wind field at "José Martí" International Airport, in Cuba. The selection of these schemes was based on their use in numerical weather forecast systems operating in Cuba. As case studies, five storms associated with synoptic patterns that cause dangerous conditions at this aerodrome were selected. The simulations were initialized at 0000 UTC with the forecast outputs of the GFS (Global Forecast System) model. The schemes were evaluated according to the representation of the wind field in the region where the airport is located, the headlands, and the center of the runway. The errors observed are strongly dependent on the occurrence of convection, especially on the intensity and the factors that cause it. During the dry season (November-April), the lowest errors are observed, while the worst performance is appreciable for the rainy period (May-October). Lin and WSM6 schemes reproduce the best behavior of the wind field on the aerodrome.

Keywords: numerical wind forecast; storms; microphysics schemes.

1. Introduction

The wind field forecast is one of the most important meteorological supports for air operations. The spatial resolution of meteorological phenomena that modifies the wind field along the runway often exceeds the range of local sensors. NWP (Numerical Weather Prediction) models are an alternative to be used as alarm systems in aeronautics [1-4].

WRF (Weather Research and Forecasting) model [5] is widely used to simulate the near-surface wind for both research and operational applications. It has two dynamic cores, the ARW (Advanced Research WRF) and the NMM (Non-hydrostatic Mesoscale Model), developed by the NCAR (National Centre for Atmospheric Research) and NCEP (National Centers for Environmental Prediction), respectively. Shaw et al. [2] implemented the WRF-ARW v2.2 model [6] for the Dubai International Airport aviation weather decision support system. The authors installed an operational system assimilating data from satellites, radiometers, wind profiles, radar, and surface observations. In the Hong Kong International Airport, a subkilometric NWP capability in capturing low-level wind

shear was evaluated [4]. This AVM (Aviation Model) [7,8] is a subkilometer resolution implementation of the WRF.

WRF model offers multiple applications, and, like most of NWP, several physics options. For wind forecast, commonly, sensitivity boundary-layer parametrizations (PBL) studies were developed [9-17]. In Cuba, the meteorological model WRF-ARW sensitivity to physics options was tested [18,19]. The predictions systems SiSPI [20] and SPNOA [21] were developed and implemented in the Center of Atmospheric Physics of the Institute of Meteorology of Cuba, but not specific to the aviation application. For this purpose, Díaz-Zurita et al. [22] improved a numerical wind surface derived from WRF-NMM for "José Martí" International Airport. This airport is located near the elevations of Cacahual. The catabatic flow modifies the characteristics of the meteorological variables at the aerodrome, and its vicinity [23]. Furthermore, at this aerodrome Sosa [24] points out that storms in the vicinity of the aerodrome usually originate dangerous phenomena associated with wind field variations.

Microphysics parametrizations are significant in predicting storms, as is described in many types of research [25-29]. In order to provide a preliminary evaluation of numerical wind field forecast over "José Martí" International Airport, a sensitivity study was developed. From WRF practice recommendations [30], ARW core was used in this research. Based on results that show the influence of storms in aerodrome vicinity wind field variations, different microphysics schemes capability to represent these changes was verified.

1.1. Study area and case studies

Barcía et al. [31] divided Cuba into forecast regions according to the behavior of the meteorological variables recorded in the observational meteorological network. The regions are classified according to the extreme temperatures, the influence of the sea breeze, and the physical-geographical characteristics. "José Martí" International Airport is located in the inland forecast region of the Artemisa, Havana, and Mayabeque provinces (Figure 1a).

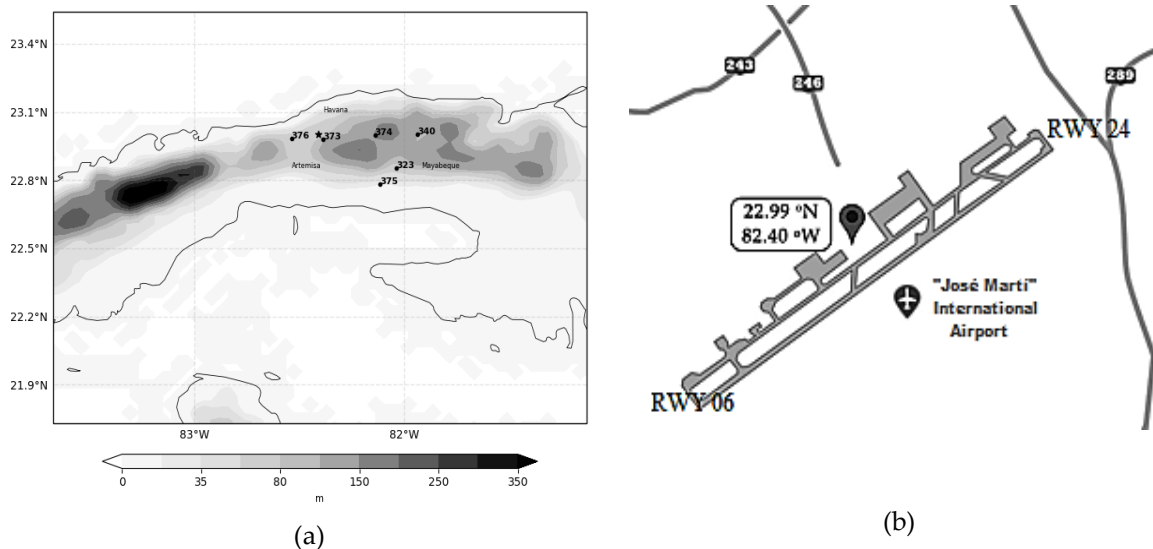


Figure 1. Study area (Artemisa–Havana–Mayabeque) (a) Topography (shaded) and meteorological observational stations (markers) (b) "José Martí" International Airport runway

This airport has a 4 km runway (Figure 1b), with southeast–northeast orientation. The airport is surrounded by terrain with complex orography. At the aerodrome, there is a catabatic flow of moist air that favors a drop in temperatures around the runway [23].

Sosa [24] used meteorological data from observations in the "José Martí" International Airport, during the period between 2012 and 2017 to describe the behavior of the low-level wind shear. This

hazardous phenomenon for aircraft is associated with meteorological systems: cold front (18.36 %), anticyclone (53.06 %), and tropical wave (10.20 %) [24]. The author identified the following synoptic patterns as the most frequent in which low-level wind shear occurs:

1. Influence of the North Atlantic Subtropical Anticyclone with trough medium and high levels.
2. Influence of the North Atlantic Subtropical Anticyclone in the entire tropospheric column.
3. Migratory anticyclones.
4. Tropical waves into the south of western Cuba.
5. Cold fronts on western Cuba.

Sosa [24] refers to that significant wind field variations over the airport are often reported under storms. As case studies, five storms associated with synoptic patterns that cause dangerous conditions at this aerodrome were selected (Table 1).

Table 1. Case studies (Synoptic patterns as the numbered list)

Date	Time (UTC)	Synoptic patterns
2012-06-29	19:01	1
2013-05-18	21:03	3
2016-07-03	20:58	4
2018-12-21	01:00	5
2019-01-27	21:58	5

2. Materials and Methods

2.1 Numerical experiments

2.1.1 Model and domain configuration

The WRF v.3.9 model was used with ARW dynamic core. The simulations comprised a 12/4 km two-way nested domains (Figure 3) and 34 verticals levels. Briefly, the setup includes for both domains: Rapid Radiative Transfer Model longwave radiation parametrization [32], Dudhia shortwave radiation scheme [33], Unified Noah land-surface model [34], Grell-Freitas Ensemble cumulus parametrization [35], Mellor-Yamada-Janjic planetary boundary layer [36]. The model was initialized and forced at the boundaries by 0.500 GFS forecast, with every 3 hourly updated boundary conditions.



Figure 2. Simulations domains.

2.1.2 Experimental design

Storms simulations were performed with four selected microphysics schemes: Lin [36], Morrison 2-moment [37], WSM5 [38], and WSM6 [39]. Table 2 shows the main species of prognostic variables in these schemes. The selection was based on their use and performance in numerical weather forecast systems operating in Cuba [18,19]. The forecasts were for 54 hours, started from the storm observation date at 0000 UTC.

Table 2. Details of the microphysics schemes considered in the study. (Y: yes, N: no) [5]

Microphysics schemes	Number of Moisture variables	Ice-Phase Processes	Mixed-Phase Processes
Lin	6	Y	Y
Morrison 2-moment	10	Y	Y
WSM5	5	Y	N
WSM6	6	Y	Y

2.2 Data and Methodology

2.2.1 Data

Wind data observations were obtained from weather stations placed in the study area (Figure 1a). The model was initialized with the GFS forecast, which is freely available at https://nomads.ncep.noaa.gov/cgi-bin/filter_gfs_0p50.pl. On the other hand, radars products were obtained from the Key West, Florida, United States (KBYX) doppler radar (available online at <https://www.ncdc.noaa.gov/nexradinv/chooseday.jsp?id=kbyx>). Also, the software NOAA Weather and Climate Toolkit v.4.5.0 (free available at <https://www.ncdc.noaa.gov/wct/install.php>) was utilized to analyze the radar data.

2.2.2 Post-processing WRF-ARW output files

In this paper, it was used the WRF-ARW output variables REFL_10CM (dBZ), T2 (K), PSFC (Pa), Q2 (kg kg⁻¹), U10 (x-component) and V10 (y-component) (m s⁻¹). Surface wind speed was computed from the output of wind components.

In the domain of 4 km (d02) of the resolution, the density of the nodes in the neighborhood of the airport is low. For this reason, the rectangular grid developed by Díaz-Zurita et al. [22] was used. This grid takes into account the orientation (60° from the horizon) and the length of the runway (4 km). Five points are marked: one in the center of the runway (MID), one at each headland, and the other two points at 1 km from the center. The grid with a longitudinal resolution of 0.87 km and a latitudinal resolution of 0.5 km is shown in Figure 3.

Based on the results of Díaz-Zurita et al. [22], for wind interpolation, the natural neighbor method was used. Also, following Díaz-Zurita et al. [22] recommendations, a correction to the interpolated wind field is applied with a consistent mass model.

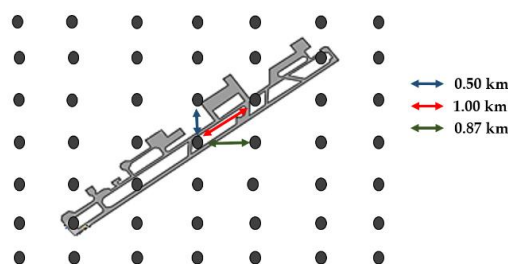


Figure 3. Rectangular grid resolution.

This model is based on the equation of continuity for an incompressible air mass moving in a two-dimensional domain, Ω , with a velocity field $\vec{u}(u, v, w)$:

$$\frac{\partial p}{\partial t} + \vec{\nabla} \cdot (\rho \vec{u}) = 0, \quad (1)$$

If the constant air density is considered for the entire domain, the equation becomes:

$$\vec{\nabla} \cdot \vec{u} = 0 \quad \text{in} \quad \Omega, \quad (2)$$

which joins the impenetrability condition on the ground Γ_b , thus constituting the boundary condition:

$$\vec{\eta} \cdot \vec{u} = 0 \quad \text{in} \quad \Gamma_b, \quad (3)$$

From conditions (2) and (3), the consistent mass models pose a least-squares problem with the velocities to adjust $\vec{u}(u, v, w)$ from the observed $\vec{u}_0(u_0, v_0, w_0)$ in the Ω domain, according to the functional:

$$E(u, v, w) = \iiint [\alpha_1^2(u - u_0)^2 + \alpha_2^2(v - v_0)^2 + \alpha_3^2(w - w_0)^2] dx dy dz, \quad (4)$$

where $\{u(x, y, z), v(x, y, z), \text{ and } w(x, y, z), \}$ are the wind components calculated by the model through fit; $\{u_0(x, y, z), v_0(x, y, z), \text{ and } w_0(x, y, z), \}$ are the components of the initial field, interpolated from the observations, and $\alpha_1, \alpha_2, \alpha_3$ are the Gaussian precision modules [40]. Considering α_1 and α_2 identical, for horizontal directions the functional to minimize (4) is:

$$E(u, v, w) = \iiint [\alpha_1^2(u - u_0)^2 + (v - v_0)^2 + \alpha_2^2(w - w_0)^2] dx dy dz, \quad (5)$$

The search field $\vec{v}(u, v, w)$ will be the solution to the problem:

Find $\vec{v} \in K$ such that,

$$E(\vec{v}) = \min_{\vec{u} \in K} E(\vec{u}), K = \{\vec{u}; \vec{\nabla} \cdot \vec{u} = 0, \vec{\eta} \cdot \vec{u}|_{\Gamma_b}\}, \quad (6)$$

This problem is equivalent to finding the saddle point at (\vec{u}, Φ) of the Lagrangian:

$$L(\vec{u}, \lambda) = E(\vec{u}) + \int \lambda \vec{\nabla} \cdot \vec{u} d\Omega, \quad (7)$$

The technique of Lagrange multipliers allows obtaining the saddle point of the expression (8), $L(\vec{u}, \lambda) \leq L(\vec{u}, \Phi) \leq L$ such that the solution field is obtained from the Euler-Lagrange equations:

$$\vec{v} = \vec{v}_0 + T \vec{\nabla} \Phi, \quad (8)$$

where Φ is the Lagrange multiplier and $T = [T_h, T_h, T_v]$ is the transmission diagonal tensor:

$$T_h = \frac{1}{2\alpha_1^2} T_v = \frac{1}{2\alpha_2^2}, \quad (9)$$

$$u = u_0 + T_h \frac{\partial \Phi}{\partial x}, v = v_0 + T_h \frac{\partial \Phi}{\partial y}, w = w_0 + T_v \frac{\partial \Phi}{\partial z}, \quad (10)$$

If α_1, α_2 are considered constant throughout the domain, the variational formulation leads to an elliptic equation defined in Φ . Indeed, substituting equation (8) in (2) results:

$$-\vec{\nabla} \cdot (T \vec{\nabla}) = \vec{\nabla} \cdot \vec{u}_0, \quad (11)$$

which is completed by the null Dirichlet condition at permeable boundaries (vertical domain boundaries)

$$\Phi = 0 \quad \text{in} \quad \Gamma_a, \quad (12)$$

and Neumann's condition in the raincoats (terrain and upper border)

$$\vec{n} \cdot \vec{\nabla} \Phi = -n \cdot \vec{v}_0 \quad \text{in} \quad \Gamma_b, \quad (13)$$

Considering T_h and T_v constant, equation (11) becomes:

$$\frac{\partial \Phi^2}{\partial x^2} + \frac{\partial \Phi^2}{\partial y^2} + \frac{T_v}{T_h} \frac{\partial \Phi^2}{\partial z^2} = \frac{-1}{T_h} \left(\frac{\partial u_0}{\partial x} + \frac{\partial v_0}{\partial y} + \frac{\partial w_0}{\partial z} \right), \quad (14)$$

eliminating the vertical component (two dimensions) was obtained:

$$\frac{\partial \Phi^2}{\partial x^2} + \frac{\partial \Phi^2}{\partial y^2} = \frac{-1}{T_h} \left(\frac{\partial u_0}{\partial x} + \frac{\partial v_0}{\partial y} \right), \quad (15)$$

This methodology guarantees the conservation of wind direction due to the impenetrability conditions.

To evaluate the radar's basic features and structure simulation of storms, verticals profiles of reflectivity and relative humidity were generated. Relative humidity was determined using Clausius-Clapeyron [41] (Equation 1)

$$RH = 0.263pq \left[\exp \frac{17.67(T-T_0)}{T-29.65} \right]^{-1}, \quad (16)$$

Where:

- T= temperature [K]
- p= pressure [Pa]
- q= specific humidity or the mass mixing ratio of water vapor to total air (dimensionless)
- T0= reference temperature (typically 273.16 K) [K]

2.2.3 Evaluation

Model output was compared with meteorological observations. In this work, the forecast verification was calculated some statistical metrics: mean systematic error or BIAS, mean absolute error (MAE), root mean squared error (RMSE), and Pearson correlation coefficient (rp). To obtain the best microphysics scheme to reproduce the surface winds properties derived from storms, the analysis was developed pre-, in- and after- the occurrence of the event [29].

3. Results and Discussion

3.1. Convective storm analysis

The late afternoon ground heat flux, the inland breeze convergence, and high-pressure levels diffluence origins the storm of June 29th, 2012. Particularly, this storm caused the highest wind speeds records on the runway. At 2:00 pm local time (18:00 UTC), the storm has a maximum height of 13.91 km and a core of maximum reflectivity of 60.5 dBZ at 4.37 km. The spatial pattern of maximum reflectivity, vertical profile mixing ratio of hydrometeor particles, and post-processed wind field were presented for tested microphysics schemes (Figure 4) in the time of storm occurred. WSM5 (Figure 4g) and WSM6 (Figure 4j) simulated high maximum reflectivity (50-55 dBZ) in the nearest location as radar did (22.978, -82.345). Both Lin and WSM6 schemes produce more than one core cloud echo. That behavior of WSM6 has been founded previously by Sari, Pulung, and Sukma [29] for a hail event study case in Surabaya, Indonesia.

The post-processed wind field for each scheme is presented, similar predicted wind speeds and directions are shown by WSM5 (Figure 4i) and WSM6 (Figure 4l). The authors reported that the microphysics schemes are not sensitive to surface properties (main wind flow in particular) and suggested a non-sensitivity of wind direction to microphysics parameterization [28,29]. However, convective storms develop are sensitive to the microphysics schemes [42-46]. In Figure 4 is shown the differences in the post-processed winds fields. The WSM5 and WSM6 wind fields are quite similar, which can be linked with the position and size of the simulated storm.

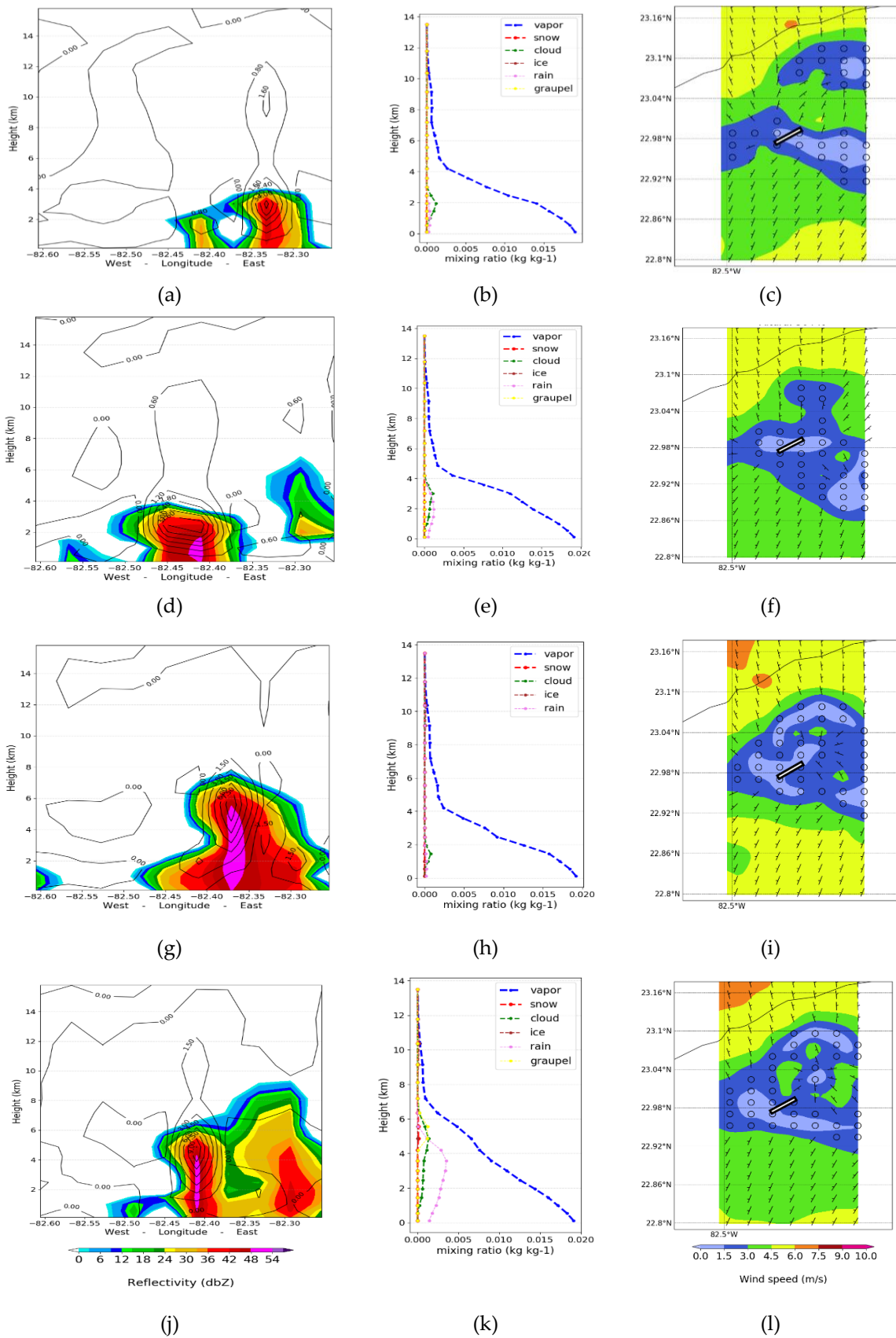


Figure 4. June 29th, 2012 storm: panels from left to right are spatial pattern of maximum reflectivity, vertical profile mixing ratio of hydrometeor particles and post-processed wind field: (a, b, c) Lin; (d, e, f) Morrison 2-moment; (g, h, i) WSM5; (j, k, l) WSM6.

Figure 4 also shows vertical simulated hydrometeor profiles; perceptible variations were observed. All schemes predict mixing ratios of hydrometeors only for warm cloud processes, which is likely to occur in Cuba. WSM6 (Figure 4k) scheme shows the best radars basics features among the schemes. In the first place, WSM6 produces more graupels than the other schemes; secondly, WSM6 presents the greatest decrease in the vapor mixing ratio near 7 km, when the rest of the diagrams show it over 5 km; and finally, WSM6 also has the highest rain mixing ratio, which decreases with increasing height, from the surface to 6 km.

3.1. Wind field simulation

Figure 5 and Figure 6 show skills metrics for forecasting wind speed and direction pre-, in- and after- the occurrence of storms selected as case studies. In the rainy season storms, for the wind speed and wind direction forecasts, the highest biases are shown in the presence of storms (Table 3). In the case studies, the occurrence of several mesoscale convective cells causes the heterogeneous distribution of the wind speed and direction.

Table 3. Rainy season biases for wind field forecast. (M.2m: Morrison 2-moment)

		Rainy season BIAS							
		Wind speed				Wind direction			
		Lin	M.2m	WSM5	WSM6	Lin	M.2m	WSM5	WSM6
Region	Pre-	1.96	2.04	1.89	1.78	-27.20	-28.33	-27.46	-24.79
	In-	1.04	1.24	1.07	0.99	-20.64	-29.18	-31.83	-28.64
	After-	1.26	1.25	1.40	1.64	21.54	8.40	15.91	26.36
Airport	Pre-	2.04	1.46	2.36	1.37	-26.91	-42.09	-54.86	-50.33
	In-	0.78	1.27	1.52	0.83	-50.51	-171.21	-157.91	-86.43
	After-	3.03	3.85	3.29	2.72	-59.90	49.82	-37.05	44.85

Also, during storms, the biggest differences in skills metrics for wind direction are obtained. This variable is underestimated. On the runway, the error measurements are more dispersed, both for speed (Figure 5d) and direction (Figure 6d). This is maybe a consequence of the different simulated storms position and characteristics from each tested microphysics. To consider the best microphysical scheme, this analysis remains difficult. However, WSM6 and Lin occasionally exhibit better scores. Previously research for this study area [47] report that WSM6 has a skill for wind forecast.

Table 4. Dry season biases for wind field forecast. (M.2m: Morrison 2-moment)

		Dry season BIAS							
		Wind speed				Wind direction			
		Lin	M.2m	WSM5	WSM6	Lin	M.2m	WSM5	WSM6
Region	Pre-	2.30	2.32	2.31	2.21	5.71	5.44	5.66	5.53
	In-	1.81	1.86	2.13	1.51	47.50	48.47	47.47	48.79
	After-	2.39	2.38	2.59	2.39	43.58	41.79	40.65	43.58
Airport	Pre-	2.94	3.31	3.77	2.62	24.24	24.24	22.45	22.17
	In-	2.70	2.85	3.33	3.25	12.93	11.76	6.93	6.42
	After-	3.23	3.28	3.70	3.45	37.82	30.76	33.83	39.16

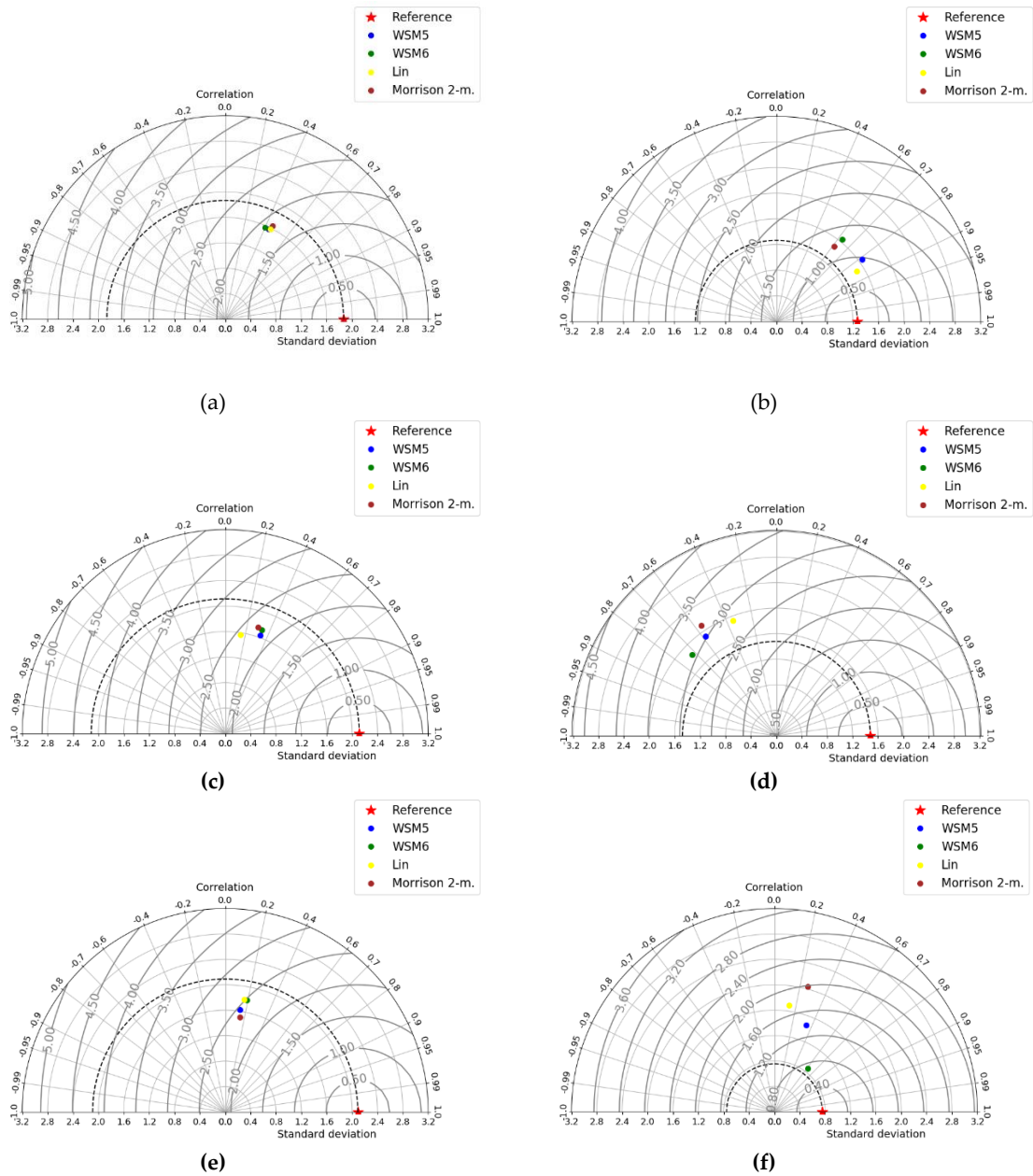


Figure 5. Taylor diagrams for rainy season wind speed forecast, panel from left to right inland region errors measurements and runway error measurements: (a, b) pre-; (c, d) in-; (e, f) after- storm.

For the dry season, the lowest biases in the wind speed forecast are observed during the occurrence of storms, as summarized in Table 4. In the case of wind direction, the highest biases are seen at this time. This behavior is similar to that observed for the rainy season. Skills metrics indicate a more accurate forecast than in the rainy season. The fundamental difference between the cases is in the origin of the storms.

In the dry season, the Pearson correlation in the region reached values of up to 0.6. On the runway, the Pearson correlations ranged between 0.7 and 0.99 (Figure 8d), which suggests the ability of the model to represent changes in wind direction, probably due to mass consistent correction applications. Once more, the schemes show fewer differences among themselves. The forecast errors may also be attributed to a lateral boundary condition; which was obtained from 0.50x0.50 horizontal resolution of the GFS forecast data.

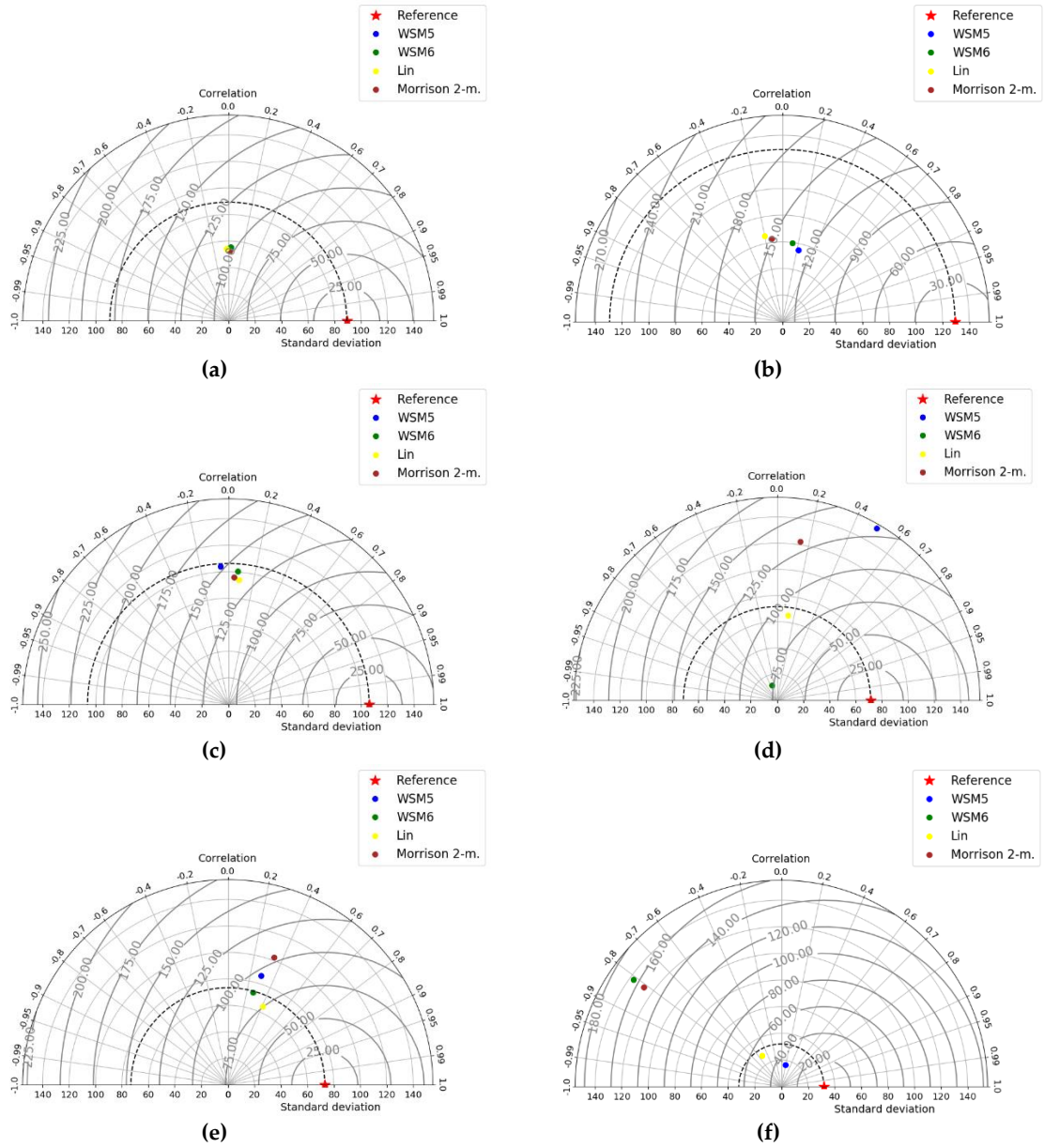


Figure 6. Taylor diagrams for rainy season wind direction forecast, panel from left to right in-land region errors measurements and runway error measurements: (a, b) pre- ; (c, d) in- ; (e, f) after- storm

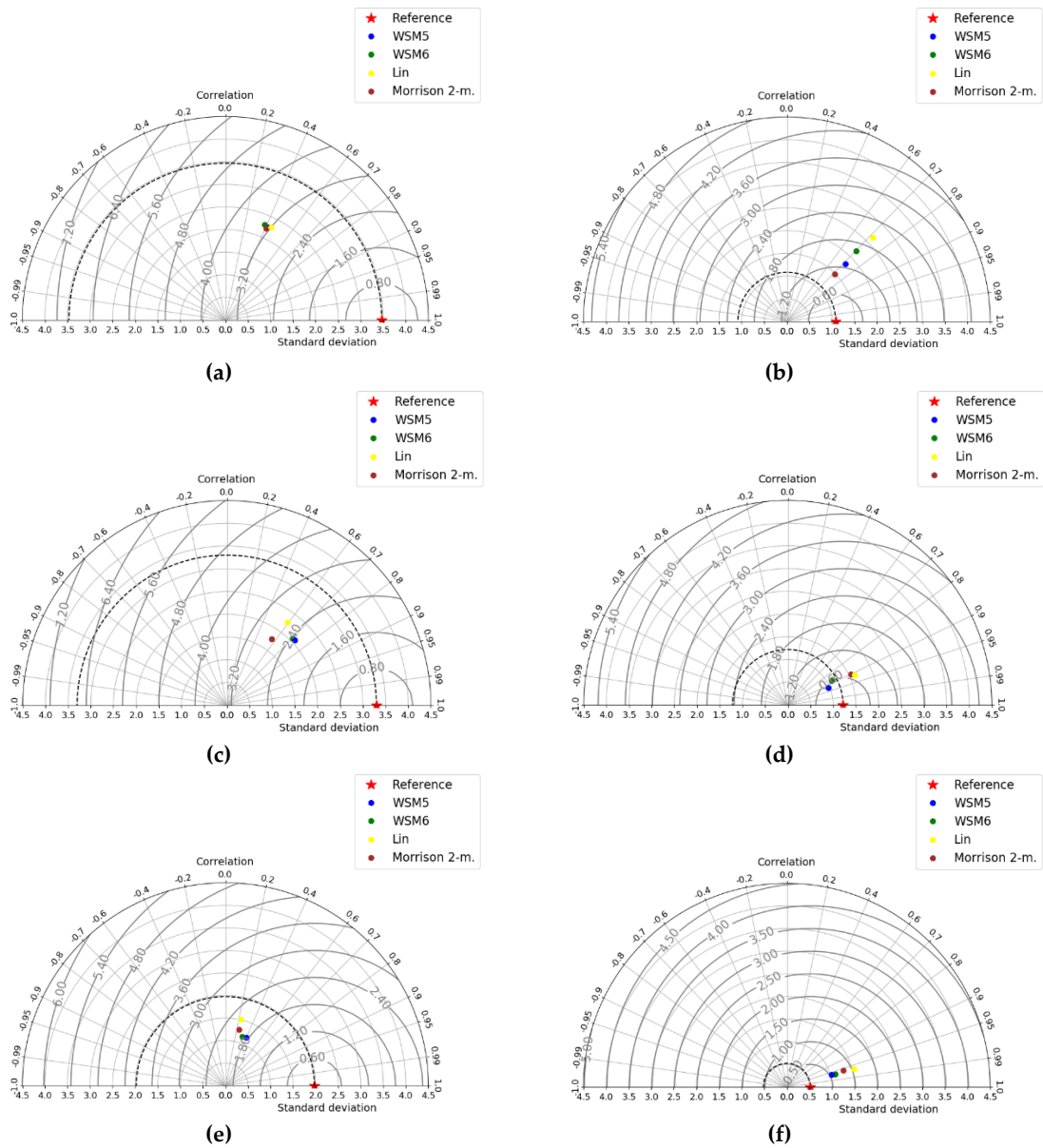


Figure 7. Taylor diagrams for dry season wind speed forecast, panel from left to right inland region errors measurements and runway error measurements: (a, b) pre- ; (c, d) in- ; (e, f) after- storm.

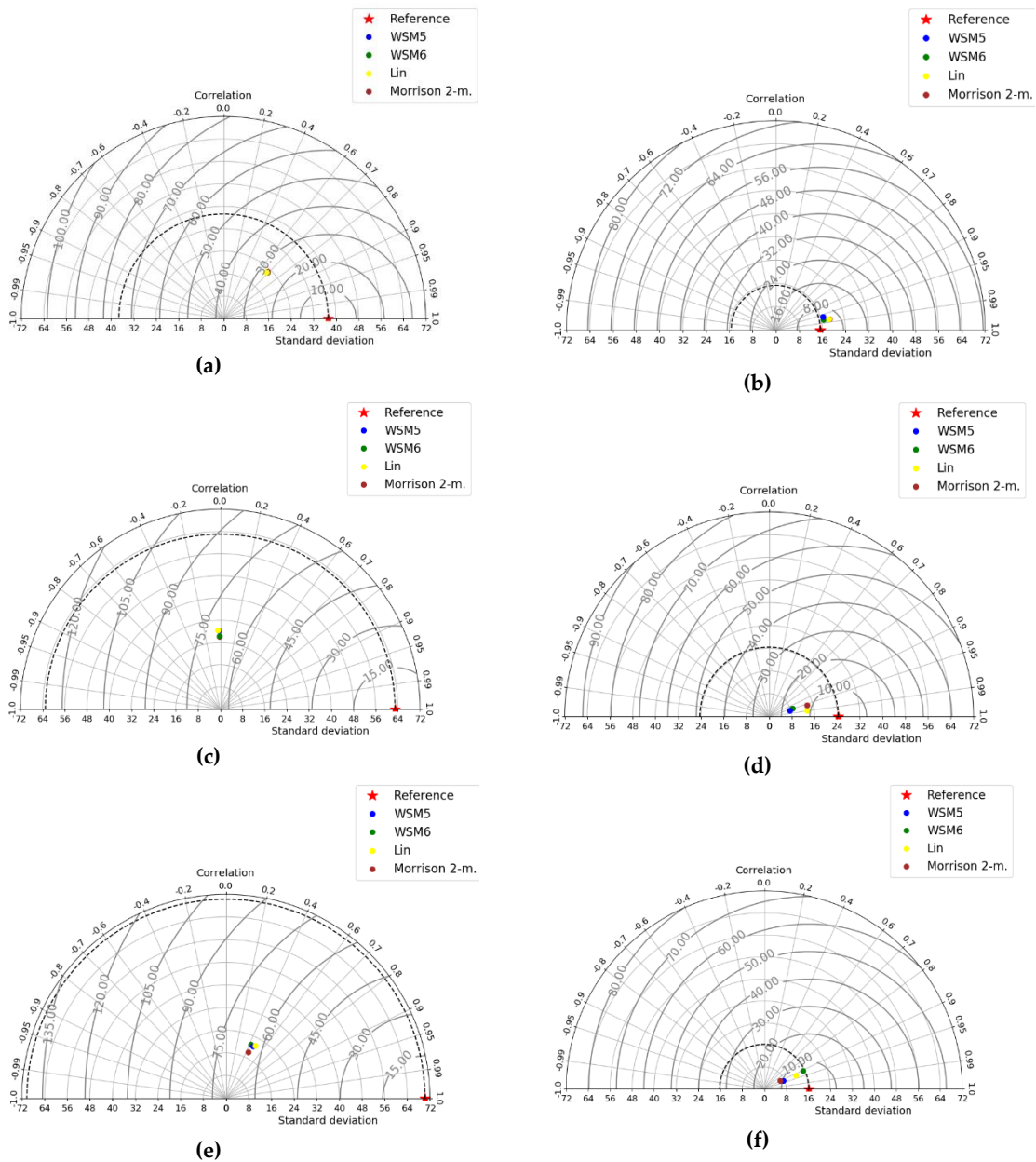


Figure 8. Taylor diagrams for dry season wind directions forecast, panel from left to right inland region errors measurements and runway error measurements: (a, b) pre- ; (c, d) in- ; (e, f) after- storm.

4. Conclusions

A sensitivity study has developed with Lin, Morrison 2-moment, WSM5, and WSM6 microphysics schemes for the numerical forecast of the wind field at "José Martí" International Airport. As case studies, five storms associated with synoptic patterns that cause dangerous conditions at this aerodrome were selected.

In section 3.1, the sensitivity of the microphysics scheme using the WRF model on June 29th, 2012, the storm has been discussed. WSM6 exhibit the most realistic storm radars features and vertical profile hydrometeors, though, all tested scheme represents distributions accord warm cloud processes, which is likely to occur in Cuba. The wind field is modified by the position and size of the simulated storms.

In section 3.2, skills metrics pre-, in- and after- storms were obtained. Between seasons was observed pronounced differences in errors, a source of errors is possibly the fact that the storms were produced from different conditions. Skills metrics indicate a more accurate forecast in dry season storms than in the rainy season ones. This study was found major correlations in wind directions forecast at the runway. A consistent mass correction application can instigate these results.

To consider the best microphysical scheme, this analysis remains difficult. However, WSM6 shows better scores in the major criterion of the study developed. Nevertheless, these results are the first attempt to obtain the best configuration of the WRF model for numerical storm forecasts in the airport. Ongoing work will therefore include other sensitivity meteorological field analysis.

Author Contributions: “Conceptualization, P.C.-H. and P.M.G.-J.; methodology, P.C.-H.; software, P.C.-H.; A.P.-A. and P.M.G.-J.; validation, P.C.-H.; formal analysis, P.C.-H.; investigation, P.C.-H. and A.P.-A.; data curation, P.C.-H. and P.G.-J.; writing—original draft preparation, P.C.-H.; writing—review and editing, P.C.-H. and A.P.-A.; visualization, P.C.-H. and A.P.-A.; supervision, A.P.-A. and P.M.G.-J. All authors have read and agreed to the published version of the manuscript.”

Funding: This research received no external funding

Acknowledgments: Authors would like to thank NOAA for freely available GFS forecast data and Key West radar data.

Conflicts of Interest: The authors declare no conflict of interest.

References

1. Boilley, A.; Mahouf, J.-F.; Lac, C. High resolution numerical modeling of low level wind-shear over the Nice-Côte d’Azur Airport. Proceedings of the 13th AMS Conference on mountain meteorology, Canada, United States of America, 2008; pp 11-15
2. Shaw, B.; Spencer, P.; Carpenter, J.; Barrere, J. Implementation of the WRF model for the Dubai International Airport aviation weather decision support system. Proceedings of the 13th Conference on Aviation, Range and Aerospace Meteorology, New Orleans, United States of America, 2008; 5.2.
3. Urlea, A.-D.; Pietrisi, M. Study of the Low Level Wind Shear using AMDAR reports. *J. Geophys. Res.* **2015**, *17*, 2015–2185.
4. Hon, K.-K. Predicting Low-Level Wind Shear Using 200-m-Resolution NWP at the Hong Kong International Airport. *J. Appl. Meteorol. Climatol.* **2020**, *59*, 193-207. [<http://doi.org/10.1175/JAMC-D-19-0186.1>]
5. Skamarock, W. C.; Klemp J. B.; Dudhia J.; Grill D.O.; Barker D. M.; Duda M.G.; Huang, X.-Y.; Wang, W.; Powers, J. G. A Description of the Advanced Research WRF Version 3, NCAR Tech Note NCAR/TN 475 STR, UCAR Communications, Boulder, Colo, 2008.
6. Skamarock, W. C.; Klemp, J. B.; Dudhia, J.; Gill, D. O.; Barker, M.; Wang, W.; Powers, J. G. A description of the advanced research WRF version 2. NCAR Tech Note NCAR/TN 468 STR, National Center for Atmospheric Research, Boulder, Colo, 2005.
7. Chan, P. W.; Hon, K.-K. Performance of super high resolution numerical weather prediction model in forecasting terrain-disrupted airflow at the Hong Kong International Airport: Case studies. *J. Meteor. Appl.* **2016**, *23*, 101-114. [<https://doi.org/10.1002/met.1534>]
8. Hon, K.-K. Simulated satellite imagery at sub-kilometre resolution by the Hong Kong observatory. *Weather* **2018**, *73*, 139–144. [<https://doi.org/10.1002/wea.3100>]
9. Srinivas C. V.; Venkatesan, R.; Bagavath Singh A. Sensitivity of mesoscale simulations of land-sea breeze to boundary layer turbulence parameterization. *Atmos. Environ.* **2007**, *41* (12), 2534-2548. [<https://doi.org/10.1016/j.atmosenv.2006.11.027>]
10. Miao J. F.; Wyser, K.; Chen, D.; Ritchie H. Impacts of boundary layer turbulence and land surface process parameterizations on simulated sea breeze characteristics. *Ann. Geophys.* **2009**, *27*, 2303-2320. [<https://doi.org/10.5194/angeo-27-2303-2009>]

11. Storm, B. and Basu, S. The WRF Model Forecast-Derived low-level wind shear climatology over the United States Great Plains. *Energies* **2010**, 3, 258–276. [<https://doi.org/10.3390/en3020258>]
12. Hu, X.-M.; Nielsen-Gammon, J. W.; Zhang, F. Evaluation of three planetary boundary layer schemes in the WRF model. *J. Appl. Meteorol. Climatol.* **2010**, 49, 1831-1844. [<https://www.jstor.org/stable/26173948>]
13. Carvalho, D.; Rocha, A.; Gómez-Gesteira, M.; Santos, C. A sensitivity study of the WRF model in wind simulation for an area high wind energy. *Environ. Model. Softw.* **2012**, 33, 23-34. [<https://doi.org/10.1016/j.envsoft.2012.01.2019>]
14. Hu, X.-M.; Klein, P. M.; Xue, M. Evaluation of the update YSU planetary boundary layer scheme with in WRF for wind resource and air quality assessments. *J. Geophys. Res. Atmos.* **2013**, 118, 10490-10505. [<https://doi.org/10.1002/jgrd.50823>]
15. García-Diez M.; Fernández, J.; Fitaand, L.; Yague, C. Seasonal dependence of WRF model biases and sensitivity to PBL schemes over Europe. *Q. J. R. Meteorol. Soc.* **2013**, 139, 501-514. [<https://doi.org/10.1002/qj.1976>]
16. Srikanth M., Satyanarayana, A. N. V.; Rao, T. N. Performance evaluation of PBL and cumulus parameterization schemes of WRF ARW model in simulating severe thunderstorm events over Gadanki MST radar facility. -Case study. *Atmos. Res.* **2014**, 139, 1-17. [<https://doi.org/10.1016/j.atmosres.2013.12.017>]
17. Boadh, R.; Satyanarayana, A. N. V. Sensitivity of PBL schemes of the WRF-ARW model in simulating the boundary layer flow parameters for their application to air pollution dispersion modeling over a tropical station. *Atmos.* **2016**, 29 (1), 61-81. [<https://doi.org/10.20937/ATM.2016.29.01.05>]
18. Sierra, M.; Borrajeró, L.; Ferrer, A. L.; Morfa, Y.; Yordanis, A.; Loyola, M.; Hinojosa, M. Sensitivity studies of the SisPI to changes in the PBL, the number of vertical levels and the microphysics and clusters parameterizations, at very high resolution. Technical Scientific Report, 2017. [<https://doi.org/10.13140/RG.2.2.29136.00005>]
19. Sánchez, E. O. Evaluation of the medium-term forecast of the atmospheric component of the SPNOA with data from INSMET meteorological stations. Bachelor Thesis, Higher Institute of Technologies and Applied Sciences, Havana, Cuba, 2018.
20. Sierra, L. M.; Ferrer, H. A. L.; Valdés, R.; Mayor, G. Y.; Cruz, R. R. C.; Borrajeró, M. I.; Rodríguez, G. C. F.; Rodríguez, N.; Roque, A. Automatic mesoscale prediction system of four daily cycles. Technical Scientific Report, 2015. [<https://doi.org/10.13140/RG.2.1.2888.1127>]
21. Pérez-Bello, A.; Mitrani, A. I.; Díaz, R. O.; Wettre, C.; Robert, L. H. A numerical prediction system combining ocean, waves and atmosphere models in the Inter-American Seas and Cuba. *Rev. Cub. Meteor.* **2019**, 25 (1), 109–120.
22. Díaz-Zurita, A.; Góngora-González, C.M; Lobaina-LaO, A.; Pérez-Alarcón. A.; Coll-Hidalgo, P. Numerical mesoscale and short-term wind forecast for the “José Martí” International Airport of Havana. *J. Braz. Meteor.* in press.
23. Grillo, N. The fog at the “José Martí” International Airport, its relationship with events and meteorological variables. Bachelor Thesis, Higher Institute of Technologies and Applied Sciences, Havana, Cuba, 2013.
24. Sosa, A. International Airport “José Martí” low-level wind shear characteristics during 2012-2017 period. Bachelor Thesis, Higher Institute of Technologies and Applied Sciences, Havana, Cuba, 2018.
25. Rajeevan, M.; Kesarkar, A.; Thampi, S.; Rao, T.; Radhakrishna, B.; Rajasekhar, M. Sensitivity of WRF cloud microphysics to simulations of a severe thunderstorm event over southeast India. *Ann. Geophys.* **2010**, 28, 603–619. [<http://doi.org/10.5194/angeo-28-603-2010>]
26. Han, J. Y.; Baik, J. J.; Khain, A. P. A numerical study of urban aerosol impacts on clouds and precipitation. *J. Atmos. Sci.* **2012**, 69(2), 504-520. [<https://doi.org/10.1007/s13143-014-0016-7>]

27. Halder, M.; Hazra, A.; Mukhopadhyay, P.; Singh, D. Effect of the better representation of the cloud ice-nucleation in WRF microphysics schemes: A case study of a severe storm in India. *Atmos. Res.* **2015**, *154*, 155-174. [<https://doi.org/10.5194/angeo-30-897-2012>]
28. Shrestha, R. K.; Connolly, P. J.; Gallagher, M. W. Sensitivity of WRF Cloud Microphysics to Simulations of a Convective Storm Over the Nepal Himalayas. *O. Atmos. Sci. J.* **2017**, *11*, 29-43. [<https://doi.org/10.2174/1874282301711010029>]
29. Sari, F. P.; Baskoro, A. P.; Hakim, O. S. Effect of different microphysics scheme on WRF model: A simulation of hail event study case in Surabaya, Indonesia. In Proceedings of the AIP Conference 2018; 020002. [<https://doi.org/10.1063/1.5047287>]
30. Dudhia, J. and Wang, J. WRF Advanced Usage and Best Practices, In 16th WRF Annual Workshop, Boulder, June 2014. https://www2.mmm.ucar.edu/wrf/users/workshops/WS2014/ppts/best_prac_wrf.pdf
31. Barcía, S.; Ballester, M.; Cedeño, Y.; García, E.; González, J.; Regueira, V. Time-space variability of the variables that intervene in short-term forecasts in Cuba. Technical Scientific Report of the Institutional Project: Evaluation of weather forecasts, 2012, 36–45.
32. Mlawer, E.J.; Taubman, S.J.; Brown, P.D.; Iacono, M.J.; Clough, S.A. Radiative transfer for inhomogeneous atmospheres: RRTM, a validated correlated-k model for the longwave. *J. Geophys. Res.* **1997**, *102*, 16663–16682. [<https://doi.org/10.1029/97JD00237>]
33. Dudhia, J. Numerical study of convection observed during the winter monsoon experiment using a mesoscale two-dimensional model. *J. Atmos. Sci.* **1989**, *46*, 3077–3107. [[https://doi.org/10.1175/1520-0469\(1989\)046<3077:NSOCOD>2.0.CO;2](https://doi.org/10.1175/1520-0469(1989)046<3077:NSOCOD>2.0.CO;2)]
34. Tewari, M., Chen, F., Wang, W., Dudhia, J., LeMone, M. A., Mitchell, K., Ek, M., Gayno, G., Weigel, J. and Cuenca, H. Implementation and verification of the unified NOAA land surface model in the WRF model. In Proceedings of the 20th Conference on Weather Analysis and Forecasting/16th Conference on Numerical Weather Prediction, Seattle, WA, USA; 17.5, pp. 11-15.
35. Grell, G. A.; Freitas, S. R. A scale and aerosol aware stochastic convective parameterization for weather and air quality modeling. *Atmos. Chem. Phys. Discuss.* **2013**, *13*, 23845–23893. [<https://doi.org/10.5194/acp-14-5233-2014>]
36. Janjić, Z. I. Nonsingular implementation of the Mellor-Yamada level 2.5 scheme in the NCEP Meso Model. NCEP Office Note 437, 2001, 61 pp.
37. Lin, Y.-L.; Farley, R. D.; Orville, H. D. Bulk parameterization of the snow field in a cloud model. *J. Climate Appl. Meteor.* **1983**, *22*, 1065–1092. [[http://dx.doi.org/10.1175/1520-0450\(1983\)022<1065:BPOTSF>2.0.CO;2](http://dx.doi.org/10.1175/1520-0450(1983)022<1065:BPOTSF>2.0.CO;2)]
38. Morrison, H.; Thompson, G.; Tatarskii, V. Impact of cloud microphysics on the development of trailing stratiform precipitation in a simulated squall line: Comparison of one- and two-moment schemes. *Mon. Wea. Rev.* **2009**, *137*, 991–1007. [<https://doi.org/10.1175/2008MWR2556.1>]
39. Hong, S.-Y.; Dudhia, J.; Chen, S.-H. A revised approach to ice microphysical processes for the bulk parameterization of clouds and precipitation. *Mon. Wea. Rev.* **2004**, *132*, 103–120. [[http://dx.doi.org/10.1175/1520-0493\(2004\)132<0103:ARATIM>2.0.CO;2](http://dx.doi.org/10.1175/1520-0493(2004)132<0103:ARATIM>2.0.CO;2)]
40. Hong, S.-Y.; Lim, J.-O. J. The WRF single-moment 6-class microphysics scheme (WSM6). *J. Korean Meteor. Soc.* **2006**, *42*, 129–151. [<https://doi.org/10.1155/2010/707253>]
41. Montero, G., Montenegro, R., Escobar, J., Rodríguez, E., and González, J. Modeling and numerical simulation of wind fields oriented to air pollution processes. University of Las Palmas, Gran Canaria, 2006.
42. Iribarne, J.V.; Godson, W.L. Atmospheric Thermodynamics. In Geophysics and Astrophysics Monographs, 2nd ed.; McCormac, B.M., Ed.; Kluwer Academic Publishers: Boston, MA, USA, 1981; pp. 259
43. Reisner, J.; Rasmussen, R.M.; Bruintjes, R.T. Explicit forecasting of supercooled liquid water in winter storms using the MM5 mesoscale model. *Q J R Meteorol Soc* **1998**, *124*, 1071-107. [<http://dx.doi.org/10.1002/qj.49712454804>]

44. Liu, C.; Moncrieff, M.W. Sensitivity of Cloud-Resolving Simulations of Warm-Season Convection to Cloud Microphysics Parameterizations. *Mon Weather Rev* **2007**, *135*, 2854-68. [<http://dx.doi.org/10.1175/MWR3437.1>]
45. Otkin, J.A.; Greenwald, T.J. Comparison of WRF Model-Simulated and MODIS-Derived Cloud Data. *Mon. Weather Rev.* **2008**; *136*, 1957-70. [<http://dx.doi.org/10.1175/2007MWR2293.1>]
46. Liu, C.; Ikeda, K.; Thompson, G.; Rasmussen, R.; Dudhia J. High-Resolution Simulations of Wintertime Precipitation in the Colorado Headwaters Region: Sensitivity to Physics Parameterizations. *Mon Weather Rev* **2011**, *139*, 3533-53. [<http://dx.doi.org/10.1175/MWR-D-11-00009.1>]
47. Rajeevan, M.; Kesarkar, A.; Rao, T.N.; Radhakrishna, B.; Rajasekhar, M. Sensitivity of WRF cloud microphysics to simulations of a severe thunderstorm event over Southeast India. *Ann Geophys* **2010**, *28*, 603-19. [<http://dx.doi.org/10.5194/angeo-28-603-2010>]
48. Coll-Hidalgo, P. International Airport "José Martí" low-level wind shear numerical forecast. Bachelor Thesis, Higher Institute of Technologies and Applied Sciences, Havana, Cuba, 2020



© 2020 by the authors. Submitted for possible open access publication under the terms and conditions of the Creative Commons Attribution (CC BY) license (<http://creativecommons.org/licenses/by/4.0/>).